Supplementary material

The tables below (Tables 2-12) give the central values of each normalised differential cross-section, and the statistical and systematic uncertainties. These tables give the normalised cross-section in each bin of the differential distribution; to calculate the numbers shown in the differential cross-section plots these cross-sections must be divided by the bin width.

In addition, Figs. 10 and 11 show the same distributions as Figs. 4 and 7, but on a linear scale for the vertical axis. Figs. 12-20 contain extra information which will be used in presentations of the analysis.

Table 2: Fraction of events contained in each bin of the jet transverse momentum distribution.

$p_{\mathrm{T}}^{\mathrm{jet}}$[GeV]	central value	statistical uncertainty	systematic uncertainty
$[10, 20]$	0.608	0.008	0.025
$[20, 30]$	0.194	0.004	0.012
$[30, 50]$	0.136	0.004	0.015
$[50, 75]$	0.043	0.002	0.006
$[75, 100]$	0.013	0.001	0.002
$[100, 150]$	0.0058	0.0007	0.0012

Table 3: Fraction of events contained in each bin of the jet pseudorapidity distribution, for $p_{\mathrm{T}}^{\mathrm{jet}} > 10$ GeV.

η^{jet}	central value	statistical uncertainty	systematic uncertainty
$[2.0, 2.5]$	0.344	0.006	0.019
$[2.5, 3.0]$	0.285	0.005	0.018
$[3.0, 3.5]$	0.215	0.004	0.016
$[3.5, 4.0]$	0.111	0.003	0.013
$[4.0, 4.5]$	0.046	0.002	0.005

Table 4: Fraction of events contained in each bin of the jet pseudorapidity distribution, for $p_{\mathrm{T}}^{\mathrm{jet}} > 20$ GeV.

η^{jet}	central value	statistical uncertainty	systematic uncertainty
$[2.0, 2.5]$	0.394	0.010	0.026
$[2.5, 3.0]$	0.309	0.009	0.023
$[3.0, 3.5]$	0.196	0.007	0.021
$[3.5, 4.0]$	0.083	0.004	0.010
$[4.0, 4.5]$	0.018	0.002	0.003

Table 5: Fraction of events contained in each bin of the Z boson transverse momentum distribution, for $p_{\mathrm{T}}^{\mathrm{jet}} > 10$ GeV.

$p_{\mathrm{T}}^{\mathrm{Z}}$[GeV]	central value	statistical uncertainty	systematic uncertainty
$[0, 10]$	0.180	0.004	0.022
$[10, 17.5]$	0.239	0.005	0.010
$[17.5, 25]$	0.200	0.005	0.007
$[25, 35]$	0.167	0.004	0.009
$[35, 50]$	0.124	0.004	0.009
$[50, 100]$	0.090	0.003	0.007

Table 6: Fraction of events contained in each bin of the Z boson transverse momentum distribution, for $p_{\mathrm{T}}^{\mathrm{jet}} > 20$ GeV.

$p_{\mathrm{T}}^{\mathrm{Z}}$[GeV]	central value	statistical uncertainty	systematic uncertainty
$[0, 10]$	0.069	0.004	0.013
$[10, 17.5]$	0.107	0.005	0.014
$[17.5, 25]$	0.164	0.006	0.017
$[25, 35]$	0.239	0.008	0.016
$[35, 50]$	0.229	0.008	0.017
$[50, 100]$	0.191	0.007	0.020

Table 7: Fraction of events contained in each bin of the Z boson rapidity distribution, y^{Z}, for $p_{\mathrm{T}}^{\mathrm{jet}} > 10$ GeV.

y^{Z}	central value	statistical uncertainty	systematic uncertainty
$[2.0, 2.5]$	0.204	0.005	0.006
$[2.5, 3.0]$	0.422	0.006	0.009
$[3.0, 3.5]$	0.315	0.005	0.008
$[3.5, 4.0]$	0.058	0.002	0.002
$[4.0, 4.5]$	0.00048	0.00017	0.00072

Table 8: Fraction of events contained in each bin of the Z boson rapidity distribution, y^{Z}, for $p_{\mathrm{T}}^{\mathrm{jet}} > 20$ GeV.

y^{Z}	central value	statistical uncertainty	systematic uncertainty
$[2.0, 2.5]$	0.231	0.008	0.008
$[2.5, 3.0]$	0.429	0.010	0.008
$[3.0, 3.5]$	0.294	0.008	0.008
$[3.5, 4.0]$	0.046	0.003	0.003
$[4.0, 4.5]$	0.00017	0.00010	0.00045

Table 9: Fraction of events contained in each bin of the $\Delta\phi$ distribution, for $p_{\mathrm{T}}^{\mathrm{jet}} > 10$ GeV.

$\lvert\Delta\phi\rvert$	central value	statistical uncertainty	systematic uncertainty
$[0, \pi/2]$	0.158	0.004	0.014
$[\pi/2, 2\pi/3]$	0.097	0.003	0.007
$[2\pi/3, 5\pi/6]$	0.196	0.004	0.008
$[5\pi/6, \pi]$	0.550	0.007	0.021

Table 10: Fraction of events contained in each bin of the $\Delta\phi$ distribution, for $p_{\mathrm{T}}^{\mathrm{jet}} > 20$ GeV.

$\lvert\Delta\phi\rvert$	central value	statistical uncertainty	systematic uncertainty
$[0, \pi/2]$	0.103	0.004	0.009
$[\pi/2, 2\pi/3]$	0.073	0.004	0.008
$[2\pi/3, 5\pi/6]$	0.169	0.006	0.007
$[5\pi/6, \pi]$	0.654	0.013	0.018

Table 11: Fraction of events contained in each bin of the Δy distribution, for $p_{\mathrm{T}}^{\mathrm{jet}} > 10$ GeV.

Δy	central value	statistical uncertainty	systematic uncertainty
$[-2.5, -1.0]$	0.086	0.003	0.006
$[-1.0, -0.5]$	0.128	0.003	0.008
$[-0.5, 0]$	0.223	0.005	0.009
$[0, 0.5]$	0.277	0.005	0.009
$[0.5, 1.0]$	0.203	0.004	0.008
$[1.0, 2.5]$	0.082	0.003	0.005

Table 12: Fraction of events contained in each bin of the Δy distribution, for $p_{\mathrm{T}}^{\mathrm{jet}} > 20$ GeV.

Δy	central value	statistical uncertainty	systematic uncertainty
$[-2.5, -1.0]$	0.057	0.004	0.006
$[-1.0, -0.5]$	0.115	0.005	0.007
$[-0.5, 0]$	0.229	0.008	0.009
$[0, 0.5]$	0.313	0.009	0.009
$[0.5, 1.0]$	0.209	0.007	0.010
$[1.0, 2.5]$	0.078	0.004	0.005

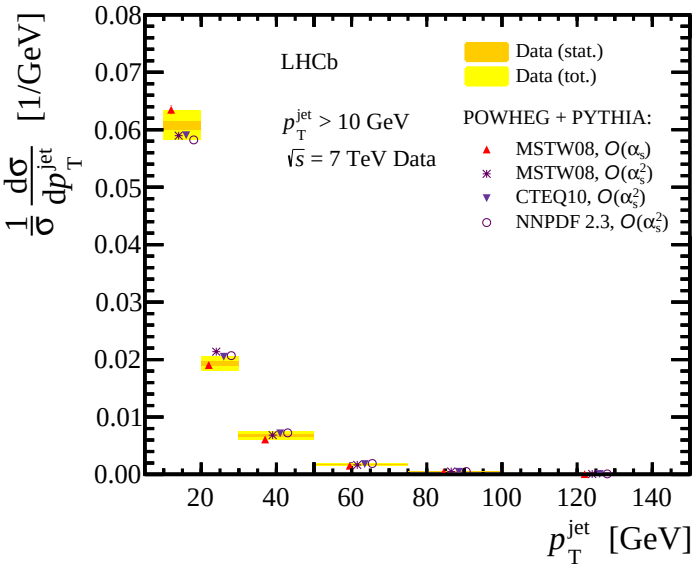

Figure 10: Cross-section for Z+jet production, differential in the leading jet $p_{\rm T}$, for $p_{\rm T}^{\rm jet} > 10$ GeV. The bands show the LHCb measurement (with the inner band showing the statistical uncertainty and the outer band showing the total uncertainty). The points correspond to different theoretical predictions with the error bars indicating their uncertainties as described in the main text. Predictions are displaced horizontally for presentation. These results are not corrected for FSR from the final state muons from the Z boson decay. This plot is the same as Fig. 4, but is shown with a linear scale for the vertical axis.

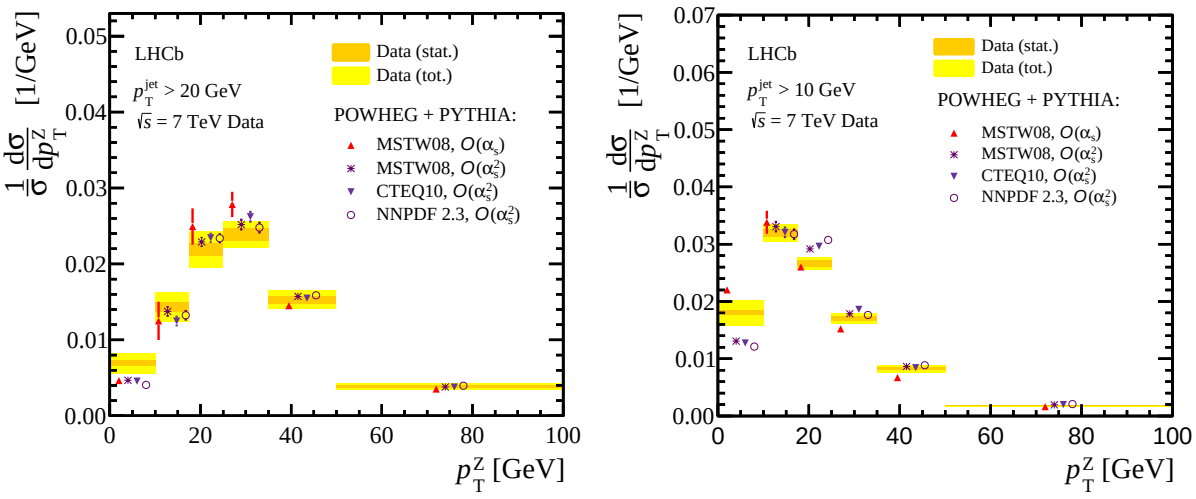

Figure 11: Cross-section for Z+jet production, differential in the Z boson transverse momentum, for (left) $p_T^{jet} > 20$ GeV and (right) $p_T^{jet} > 10$ GeV. The bands show the LHCb measurement (with the inner band showing the statistical uncertainty and the outer band showing the total uncertainty). Superimposed are predictions as described in Fig. 4. The plots are the same as Fig. 7, but are shown with a linear scale for the vertical axis.

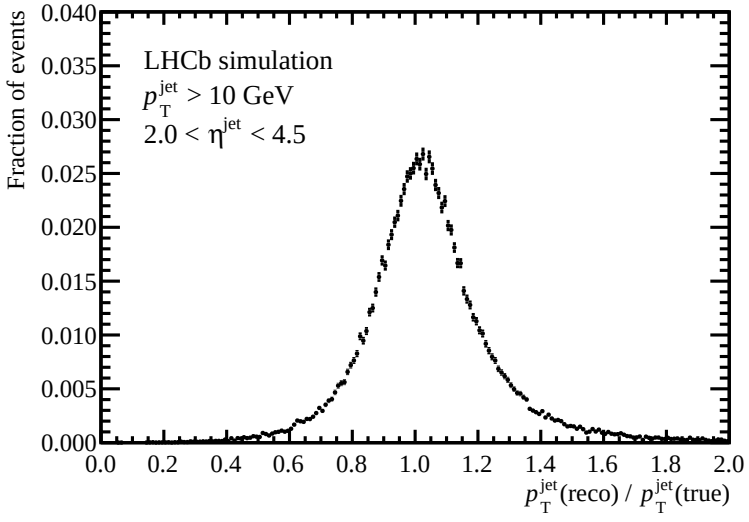

Figure 12: Resolution of the jet transverse momentum in LHCb simulated data.

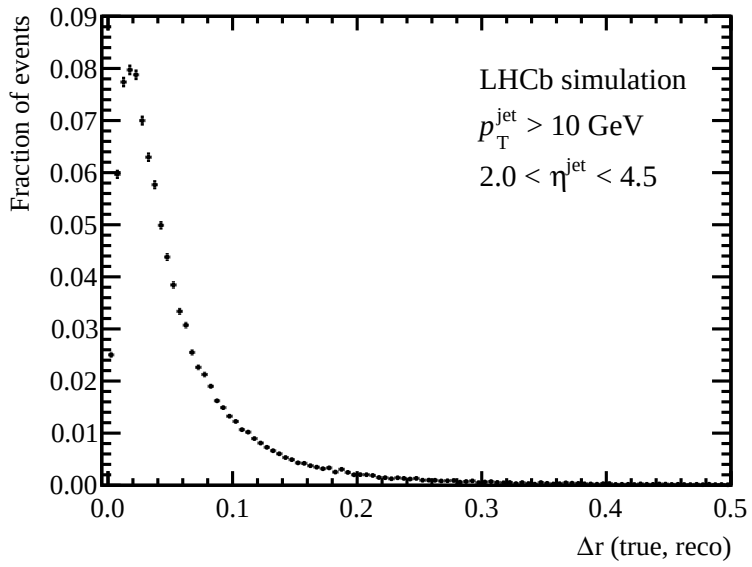

Figure 13: Resolution of the jet direction in LHCb simulated data.

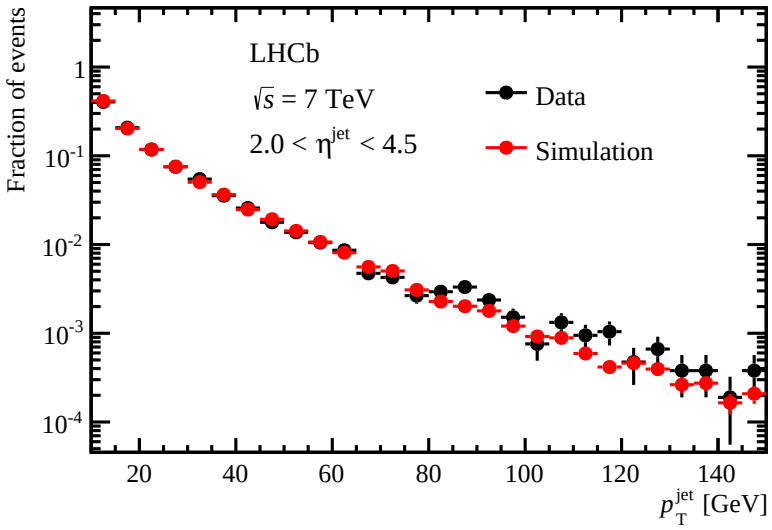

Figure 14: Reconstructed jet transverse momentum distribution in data and the LHCb simulation. No corrections for detection efficiencies or resolution effects have been made, and the histograms are normalised to have unit integral.

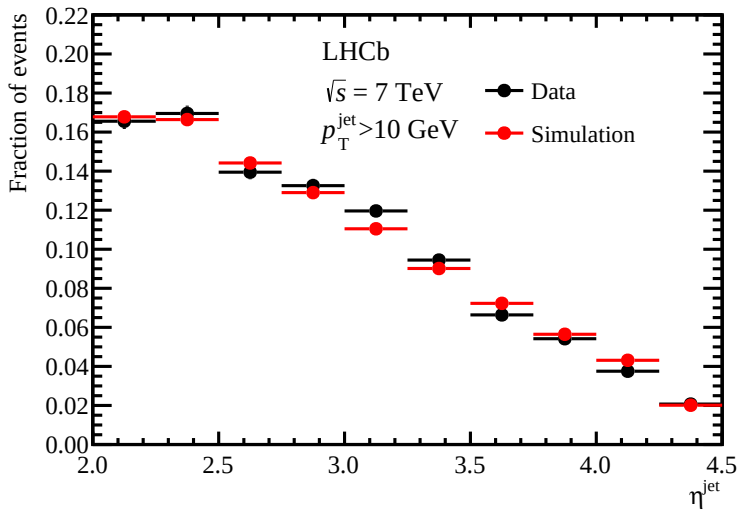

Figure 15: Reconstructed jet pseudorapidity distribution in data and the LHCb simulation. No corrections for detection efficiencies or resolution effects have been made, and the histograms are normalised to have unit integral.

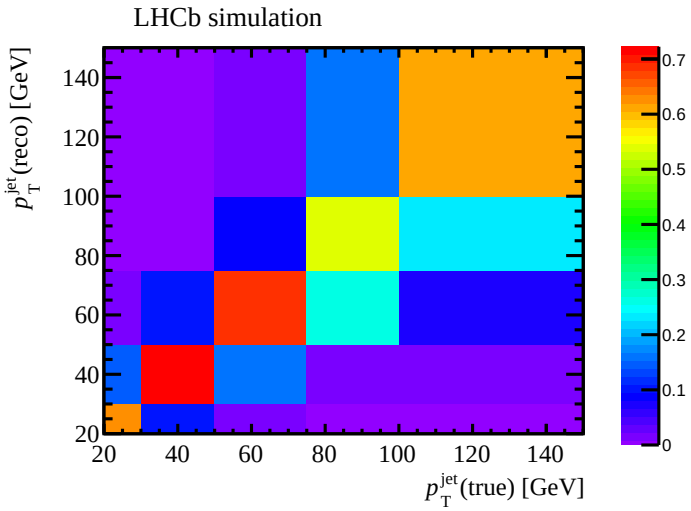

Figure 16: Probability that an event with a given true p_T of the leading jet (horizontal axis) is reconstructed in a particular bin of the measured jet p_T (vertical axis). Columns therefore sum to one. This probability is shown by the colour scheme.

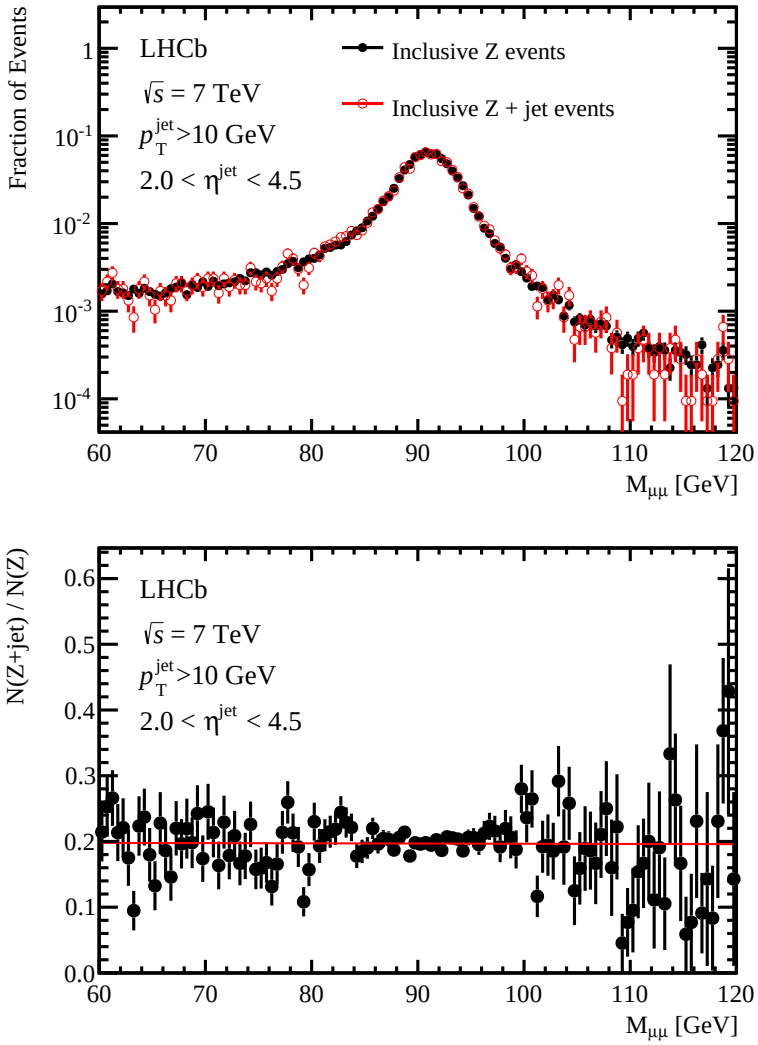

Figure 17: (Top) Invariant mass distributions of dimuon candidates for inclusive Z (black) and inclusive Z+jet (red) events, where both distributions are normalised to have unit integral. (Bottom) Ratio of the number of Z+jet events to the number of inclusive Z events as a function of the invariant mass of the dimuon pair. The distribution is fit with a straight line, which is consistent with having zero gradient.

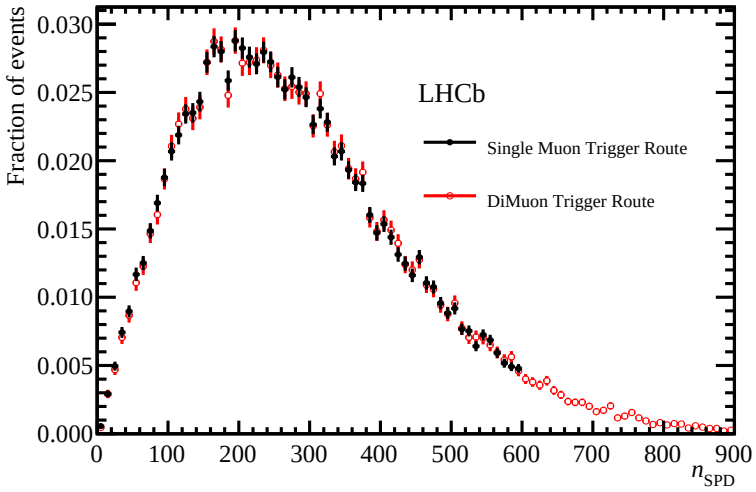

Figure 18: Number of SPD hits, n_{SPD}, for the two different trigger routes considered in this analysis.

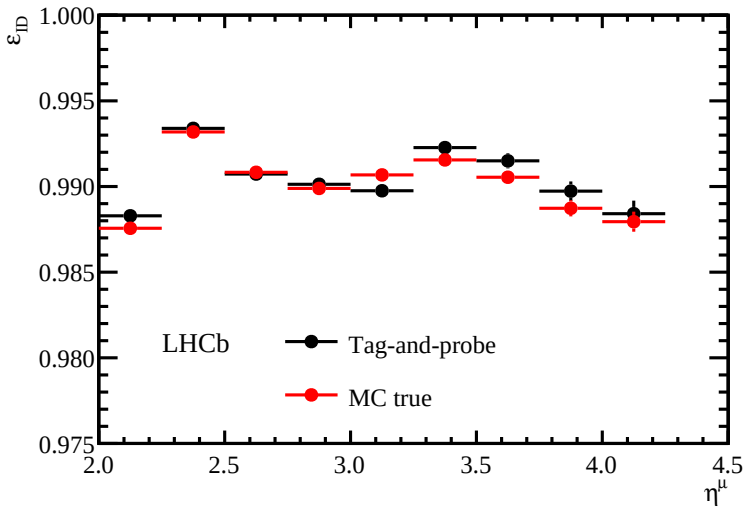

Figure 19: Muon identification efficiency measured using the tag-and-probe method on simulation and the true efficiency determined directly from simulation. These were determined on statistically independent samples.

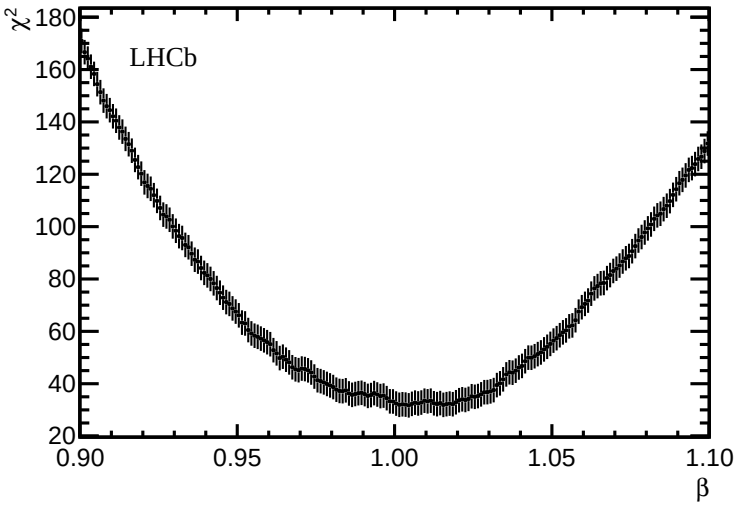

Figure 20: Detector response to jets is varied by a factor β in simulation, and the consistency with data is measured using a χ^2 comparison of the distribution shown in Fig. 2. The best value of β is consistent with unity, corresponding to the nominal detector response in the LHCb simulation.